International Journal of
Turbomachinery
Propulsion and Power

MDPI

Article

Aerodynamics of Short Intake at High Incidence †

Fernando Tejero [1,*], David MacManus [1], Josep Hueso-Rebassa [1], Yuri Frey Marioni [2] and Ian Bousfield [2]

[1] School of Aerospace, Transport and Manufacturing, Cranfield University, Bedford MK43 0AL, UK
[2] Rolls-Royce plc, P.O. Box 31, Derby DE24 8BJ, UK
* Correspondence: f.tejero@cranfield.ac.uk
† This article is a revised and expanded version of a paper entitled "Aerodynamics of a Short Intake at High Incidence", which was presented at 16th European Turbomachinery Conference, ETC2025, Hannover (Germany), 24–25 March 2025.

Abstract

This work assesses the aerodynamics of a short aero-engine intake for a new rig that is planned to be tested at the Large Low-Speed Facility of the German Dutch Wind Tunnels (LLF-DNW) in 2025. A range of computations were performed to assess whether the expected aerodynamics in this arrangement encompass the envisaged range of flow field characteristics of the equivalent isolated configuration. The effect of massflow capture ratio and angle of attack are investigated. In addition, an intake flow separation taxonomy is proposed to characterise the associated flows. The wind tunnel analysis is based on two different modelling approaches: an aspirated isolated intake and a coupled fan–intake configuration. The coupled configuration uses a full-annulus model with a harmonic mixing plane method. Across the range of operating conditions with changes in the massflow capture ratio and angle of attack, there are attached and separated flows. The main separation mechanisms are diffusion-driven and shock-induced, which shows the different aerodynamics that may be encountered in a short intake. Overall, this work provides an initial evaluation of the aerodynamics of the new fan/intake test rig configuration, provides guidance for wind tunnel testing, and lays a foundation for subsequent unsteady coupled fan–intake studies.

Keywords: intake; fan coupling; high incidence

1. Introduction

Within the context of civil aero-engines for podded under-wing configurations, increasing the bypass ratio [1] and reducing the fan pressure ratio can lead to improved propulsive efficiency and reduced fuel burn [2,3]. Although this can be achieved by an increase in fan diameter, the potential drag and weight penalty from a conventionally designed intake [4], nacelle [5], and exhaust [6] may erode the performance benefits from the low specific thrust cycles [7]. For this reason, it is expected that future civil aero-engines will use compact housing components [8,9]. Consequently, a key consideration is the design of short intakes and intake/fan compatibility under off-design conditions such as crosswind [4] or high incidence [10]. There are aerodynamic design challenges associated with this new design space, such as the reduced diffusion capability of short intakes or the expected larger accelerations around the lip in which shock wave boundary layer interaction could occur. In addition, the greater coupling with the fan requires computational methods that model the fan–intake interaction to properly assess its aerodynamic performance. Previous research shows that under crosswind and high-incidence conditions, the fan can reduce the flow distortion and

Check for updates

Academic Editor: Marcello Manna

Received: 2 June 2025
Revised: 23 October 2025
Accepted: 3 December 2025
Published: 5 January 2026

Copyright: © 2026 by the authors. Published by MDPI on behalf of the EUROTURBO. Licensee MDPI, Basel, Switzerland. This article is an open access article distributed under the terms and conditions of the Creative Commons Attribution (CC BY-NC-ND) license.

increase the critical crosswind velocity [11] and critical angle of attack [12], respectively. A range of different modelling approaches to account for the fan rotor have been considered in the past. This includes computationally expensive full-annulus configurations where the geometries of the rotating fan and stationary downstream components are included and low-order methods such as body force models (BFMs) [13] and Actuator Discs (ADs) [14].

Previous studies have investigated the feasible design space for short intakes under high-incidence conditions. Peters et al. [15] developed a CFD methodology in which the fan was modelled with a simplified body force model. A range of short intakes were considered, in which the ratio of the intake length (L_{int}) to the fan diameter (D_{fan}) was varied between L_{int}/D_{fan} = 0.19 and 0.5. This is defined as a short design since it is below the typical range for current intakes that are between L_{int}/D_{fan} = 0.5 and 0.65 [15] . Whilst shortening the intake yielded nacelle drag benefits under mid-cruise conditions, it was concluded that $L_{int}/D_{fan} < 0.25$ was not feasible due to the reduction in fan efficiency at high incidence climb-out caused by local flow separation at the fan face. Cao et al. [10] performed a numerical study on the fan/intake interaction under high incidence with a BFM. The impact of intake length on flow separation and distortion was investigated. It was determined that for a short intake with L_{int}/D_{fan} = 0.17, the last angle of attack at which the flow is attached to the intake bottom aero-line could be increased by approximately 5° relative to an aspirated configuration in which the effect of the fan is not considered. However, it is important to note that this is probably an unfeasible part of the intake design space due to the expected reduction in fan efficiency identified by Peters et al. [15]. For an intake with L_{int}/D_{fan} = 0.44 operating under high-incidence conditions, it was shown that whilst the fan did not impact the critical angle of attack at which there was separation, the fan reduced the intake distortion post-separation. Kennedy et al. [16] also investigated the fan/intake interaction under high incidence, for which low-order models were not used, and a full-annulus 3D fan geometry was considered. Their work was based on a conventional long intake with $L_{int}/D_{fan} > 0.6$ at M = 0.25 and a massflow capture ratio ($MFCR$) of approximately 1.5. This $MFCR$ is typical of take-off conditions under high incidence [17]. It was concluded that the effect of the fan resulted in an increment in the critical angle of around 1° compared with a case without it. Carnevale et al. [18] conducted a computational study on flow separation in a subsonic civil aircraft intake with $L_{int}/D_{fan} \approx 0.6$. Steady RANS simulations were conducted for an aspirated case and unsteady RANS computations for a powered intake configuration. It was reported that the fan stage improves the tolerance to variations in flow incidence and effectively reduces flow distortion. For this intake configuration, the fan/intake interaction resulted in an increment in the critical angle by 5° relative to the aspirated case. Magrini et al. [19] performed a parametric study of geometric intake design variables to assess their impact on flow distortion. Their work was based on a short intake with L_{int}/D_{fan} = 0.35 coupled with a body force model at M = 0.25 and $MFCR$ = 1.55. It was concluded that the contraction ratio has a large impact on inlet separation. Relative to cases without a fan model, the BFM resulted in a larger separation suppression and, therefore, higher critical angles. Gunn et al. [20] investigated the intake performance of a short configuration with L_{int}/D_{fan} = 0.34 at high incidence. Their study was based on aspirated and coupled fan/intake configurations. For the coupled arrangement, the fan, outlet guide vane, and engine section stator were modelled with a mixing plane approach. It was determined that the critical angle of attack increased by approximately 2° due to the effect of the fan.

The majority of previous work in flow distortion for civil aero-engine intakes is based on computational methods with a range of different modelling approaches. They highlight the strong fan/intake interaction and showcase that aspirated configuration may lead to

unphysical results due to the neglected coupling effect. Nevertheless, its impact on the intake performance varies between studies, where the change in critical angle between aspirated and intake/fan coupled cases can range from 1° [16] to 5° [10]. Whilst these can be the result of using different intake shapes, thus making the associated aerodynamics different, it could also be related to the modelling approaches used. For this reason, it is important to validate the numerical methods for aero-engine intake applications. However, there is very limited information in the open literature for experimental work. Coschignano et al. [21,22] conducted a canonical 2D experimental study of shock wave boundary layer interaction (SBLI) on the intake lip under take-off conditions. The changes in the shock characteristics and onset of flow separation as a function Reynolds number, angle of attack, and lip shape were investigated. It was concluded that boundary layer separation was very sensitive to the SBLI topology. Hodder [23] carried out measurements to investigate the fan effect on intake performance for a model-scale configuration with a fan diameter of 44 in (111.8 cm) and a long intake of $L_{int}/D_{fan} > 0.6$. It was found that the fan interaction allows the intake to operate with lower distortion levels at and above the critical angle that the intake would experience without the fan interaction.

There is a clear research gap in characterising the intake aerodynamics of short configurations across a range of operating conditions using measurements. Collecting this data would not only provide valuable insights into intake distortion characteristics but also serve as a crucial validation test case for CFD methods. This could significantly improve the understanding and prediction of intake performance, particularly in complex flow conditions, enhancing future aero-engine intake design and optimisation methods. Within this context, a significant research programme is in development for the experimental testing and evaluation of a novel short fan/intake configuration. The experiments will be performed at the Large Low-Speed Facility of the German Dutch Wind Tunnels (LLF-DNW). This work is predominately an assessment of the intake aerodynamics through a pre-test CFD analysis of the fan/intake test rig configuration. It is an initial part of the development programme, and the results will inform the design and setup of the test campaign which is planned for 2025.

2. Methodology

A computational model was developed for the investigation of the aerodynamics of a short intake rig with D_{fan} = 14 in (0.36 m) that will be installed at LLF-DNW [24]. It is a non-axisymmetric intake that is representative of future civil aero-engines with $L_{int}/D_{fan} = 0.33$. This work is based on a high-incidence arrangement at a nominal freestream Mach number of 0.25. Two different configurations are considered: an aspirated intake in which the effect of fan interaction is neglected and a fan–intake coupled analysis with a full-annulus computational approach (Figure 1).

Due to the relatively complex geometry of the full wind tunnel arrangement that includes the wind tunnel geometry, rig, intake, and turbomachinery components, an overset grid approach was used. The computational domain was divided into 4 independent sub-domains: wind tunnel, rig, intake, and turbomachinery (Figure 2). The turbomachinery sub-domain contains the rotating fan as well as the stationary downstream components of outlet guide vanes (OGVs) and wind tunnel struts (Figure 1). These stationary components are included as they can affect the flow distortion at the intake [25]. The overset grid approach enables the simulation of different intake incidence angles by imposing changes in the relative angle between the wind tunnel and the rig/intake/turbomachinery sub-domains. The grids for the wind tunnel and rig were created with a hybrid meshing approach using a structured prism layer near the viscous walls and $y^+ \approx 50$. Unstructured tetrahedral elements were used in the rest of the domain. The intake and turbomachinery

meshes used a multi-block structured meshing approach with a $y^+ = 1$. The spatial discretisation of the wind tunnel, rig, and intake meshes was based on a grid sensitivity study of the aspirated configuration (Figure 1). Overall, three different mesh levels were considered (Table 1). For an attached flow condition with a massflow capture ratio ($MFCR$ as defined in Equation (1)) of approximately 1.6 and an incidence angle of 1° below the critical angle, i.e., $AoA = AoA_{crit} - 1°$, the grid convergence index [26] of the medium mesh was 2.1% and 0.05% based on DC_{60} and the peak isentropic Mach number along the bottom intake aero-line. In addition, the impact of spatial resolution on predicting the critical angle of attack was studied. For this purpose, an incidence sweep was performed with a resolution of 1° at a fixed $MFCR \approx 1.6$. It was determined that the medium and fine meshes have the same critical angle and similar intake distortion metrics post-separation (Figure 3). Based on this, the medium meshes of the wind tunnel, rig, and intake sub-domains, which have a total of 108.6×10^6 cells, were selected for this work. The spatial discretisation of the turbomachinery elements, i.e., fan, OGVs, and struts, was based on previous guidelines [27]. Overall, the full annulus for the fan, OGVs, and strut meshes were composed of 75.0×10^6, 78.0×10^6, and 8.0×10^6 cells, respectively. This results in an overall cell count of the wind tunnel arrangement for the fan–intake coupled analysis of approximately 269.0×10^6 cells.

$$MFCR = \frac{A_\infty}{A_{hi}} = \frac{\dot{m}_{fan}}{\rho_\infty U_\infty A_{hi}} \tag{1}$$

where $\dot{m}_{fan}$ is the massflow through the fan, ρ_∞ is the density at the inlet of the working section, U_∞ is the velocity at the inlet of the working section, and A_{hi} is the intake highlight area.

Table 1. Grid levels for mesh sensitivity study of aspirated arrangement.

Component	Coarse	Medium	Fine
Wind tunnel	30.0×10^6	64.1×10^6	126.0×10^6
Rig	13.4×10^6	27.1×10^6	51.6×10^6
Intake	8.6×10^6	17.4×10^6	32.8×10^6
Total	52.0×10^6	108.6×10^6	210.4×10^6

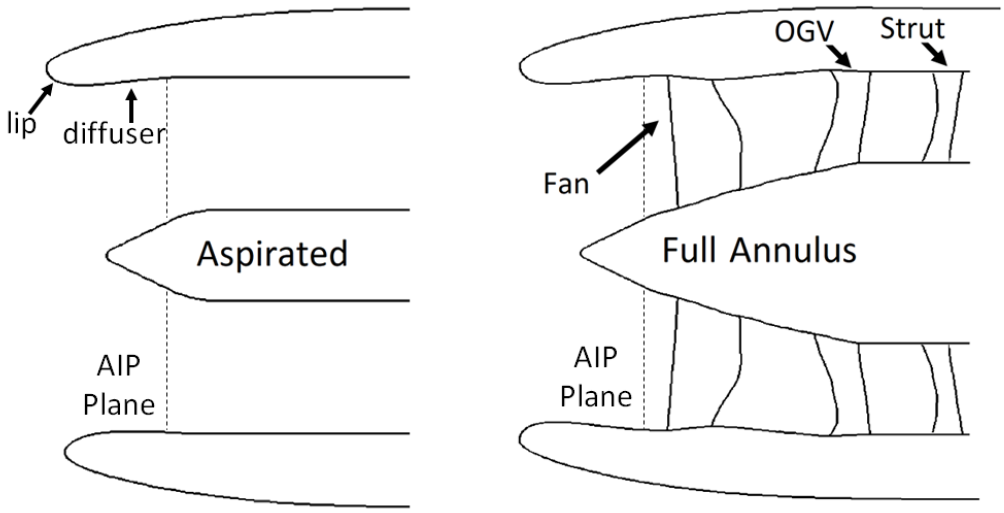

Figure 1. Overview of intake modelling: Aspirated intake (**left**) and fan–intake coupled arrangement (**right**).

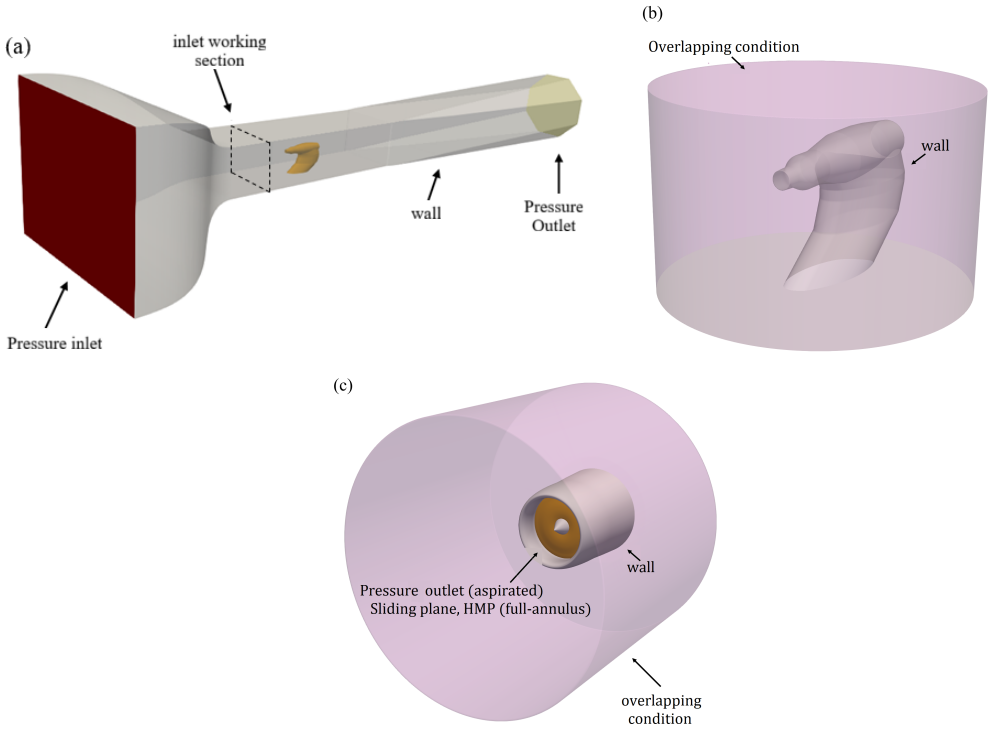

Figure 2. (**a**) LLF-DNW wind tunnel sub-domain. Rig surface is included for reference for overall size. (**b**) Rig sub-domain. (**c**) Intake sub-domain.

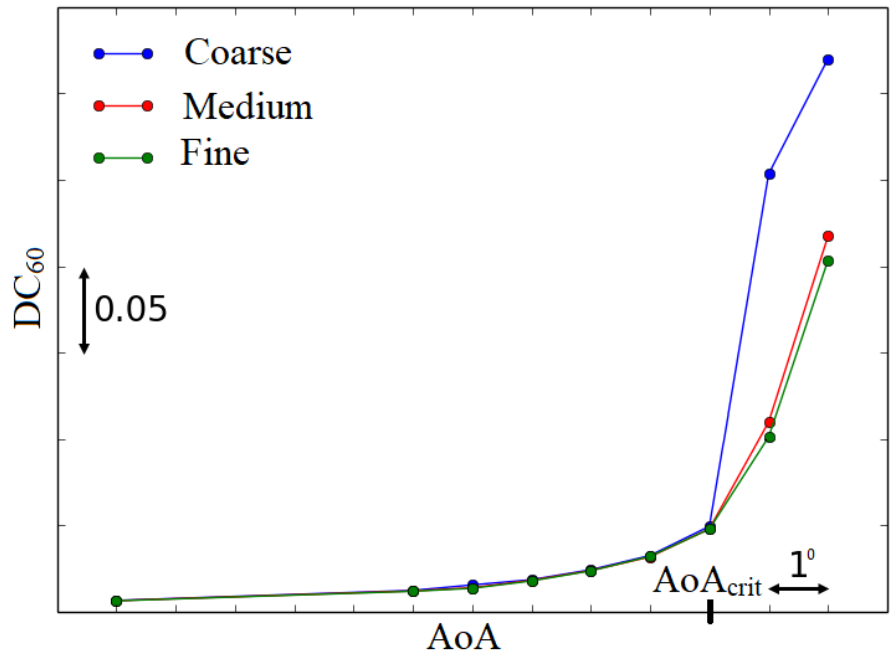

Figure 3. Changes in DC_{60} as a function of angle of attack for the 3 different grid levels.

The simulations were performed with the finite volume solver HYDRA [28]. It solves the compressible steady Favre-averaged Navier–Stokes equations with a double precision, implicit density-based approach. The turbulence model k-ω SST [29] was used for all the simulations, and the spatial discretisation was defined with a second-order MUSCL scheme [30]. The Green–Gauss method was used for the calculation of the gradients [31] and Sutherland's law for dynamic viscosity [32]. An automatic Spalding blended wall function method was employed [28]. For this approach, the blending function is deactivated when y^+ is below 5. Conversely, the blending method is activated for larger y^+ values and uses wall

functions to model the boundary layer. The inlet of the wind tunnel domain was defined with a pressure inlet boundary condition in which the total pressure and temperature were prescribed. The outlet of the wind tunnel used a pressure outlet condition with a target massflow. The value of the massflow was defined to achieve the desired velocity at the entry of the working section (Figure 2a). As part of this work, this was set to a nominal Mach number of 0.25. All the walls of the wind tunnel, rig, intake, and turbomachinery sub-domains used a viscous no-slip wall condition and were modelled as smooth walls. An overlapping boundary condition was set for the external boundary of the rig grid to link the wind tunnel and rig sub-domains. This approach was previously validated by Amirante et al. [33,34]. Similarly, the external boundaries of the intake mesh used an overlapping condition to connect the rig and intake meshes. For the aspirated arrangement, a simplified annular duct was added after the nominal fan face and the engine massflow was controlled with a pressure outlet boundary. To provide insights into the aerodynamics of the installed arrangement, an example of a CFD solution for the aspirated configuration at M = 0.25, $AoA = AoA_{crit} - 1°$, and $MFCR \approx 1.6$ is presented in Figure 4. The fan–intake coupled analysis uses full-annulus computations with a harmonic mixing plane (HMP) approach between the interfaces of the turbomachinery elements. The HMP method is based on an adaptation in the frequency domain of the filtering mixing plane technique proposed by Pullan and Adamczyk [35]. Relative to the standard mixing plane formulation, the HMP retains low-order spatial frequencies to obtain more accurate steady solutions. It also provides a better initialisation for future URANS calculations. For all simulations, iterative convergence was a reduction in normalised residuals of approximately four orders of magnitude. In addition, the solutions had a maximum oscillation of inlet massflow of 0.25% over the last 500 iterations.

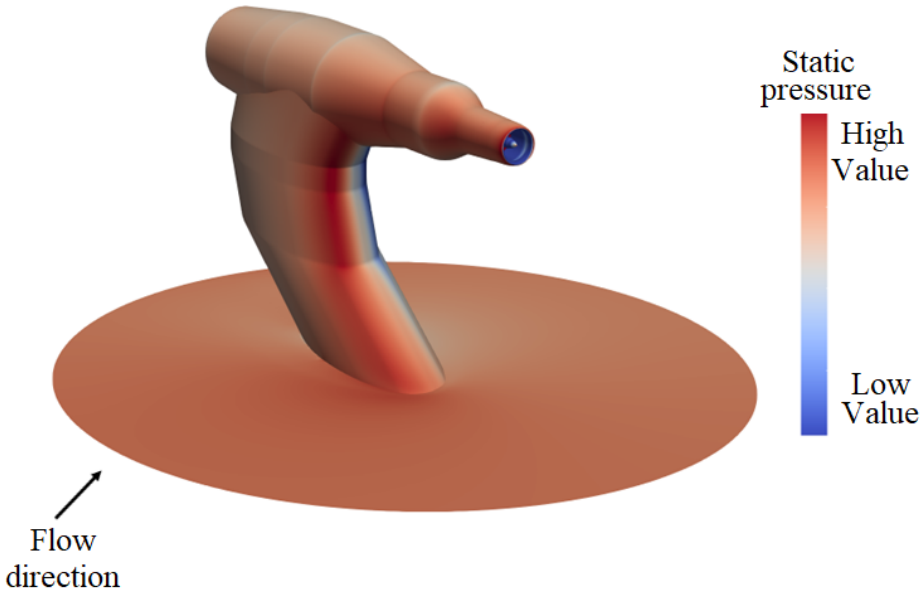

Figure 4. An example of the CFD solution for the installed aspirated configuration (rig and intake sub-domains) at M = 0.25, $AoA = AoA_{crit} - 1°$, and $MFCR \approx 1.6$.

3. Results

As discussed above, this work presents the initial phase of a broader development program that involves a comprehensive test campaign of a short aero-engine intake. To achieve the goals of the development program, three key activities were undertaken [24]. The first focus was to assess the intake aerodynamics of the installed LLF-DNW configuration and determine how accurately it can reflect the flow characteristics of an isolated

intake (Section 3.1). This evaluation was required to ensure that the aerodynamic data from the wind tunnel configuration will be representative of short aero-engine intakes. Following this initial consideration, a detailed investigation into the intake aerodynamics was conducted across a range of massflow capture ratios and incidence angles to evaluate the expected flow distortion characteristics and flow separation mechanisms (Section 3.2). Lastly, the coupling between the intake and the fan was examined to assess its impact on the intake distortion response (Section 3.3).

3.1. Comparison Between Isolated and Installed LLF-DNW Intake Aerodynamics

An initial analysis was performed to identify whether the installed intake aerodynamics in the LLF-DNW are representative of an isolated configuration. The isolated arrangement excludes the wind tunnel and rig, and its domain resembles the one shown in Figure 2c, with the overlapping conditions replaced by a far-field condition and shifted further away. For this work, this study focused on the aspirated arrangement (Figure 1) because it is sufficient to capture the upstream potential flow of the intake and identify changes that might be introduced by the test rig. The analysis was undertaken for a representative $MFCR \approx 1.6$ across a wide range of angles of attack in which the flow is attached and separated. The CFD simulations showed that the flow blockage induced by the rig caused a change in the upwash angle. For this reason, an incidence angle correction was derived to compare installed and isolated cases at the same effective incidence angle, i.e., the upwash angle is accounted for. All the comparisons between the isolated and installed arrangements presented below include the incidence correction. Therefore, both configurations have a similar effective angle of attack. It is important to note that although the wind tunnel correction was derived and validated for a fixed intake geometry, it is anticipated that modest variations in the intake geometry will not significantly impact the correction because it is predominantly influenced by the rig blockage. However, this was not proven, as this work was limited to a single intake configuration. At zero incidence, the geometric blockage of the intake in the tunnel working section, based on the nacelle forebody maximum diameter, is approximately 0.3%. The distance between the intake and the wind tunnel walls is around $11 \cdot D_{fan}$. This is reduced to $7 \cdot D_{fan}$ for the maximum considered angle of attack. The verification of the flow similarities between installed and isolated arrangements is considered in terms of the aerodynamics along the intake surface, flow characteristics at the Aerodynamic Interface Plane (AIP in Figure 1), and intake distortion metrics. The AIP was positioned $0.05 \cdot D_{fan}$ upstream of the blade hub leading edge.

For incidence angles without a large open flow separation, there is an excellent agreement in terms of the isentropic Mach number along the intake between the installed LLF-DNW and isolated configurations. Figure 5 shows the M_{is} distributions along the intake bottom ($\psi = 180°$) and bottom-control ($\psi = 135°$) aero-lines at an angle of attack one degree below the critical incidence ($AoA = AoA_{crit} - 1°$). The differences between both configurations in terms of peak and pre-shock M_{is} is within 0.02, and the shock location is within $\Delta X / L_{int} = 0.005$. For separated flows, i.e., angles of attack above AoA_{crit}, larger changes emerged due to the inherent challenges associated with modelling these flows in RANS simulations. The typical values and distributions of the isentropic Mach number along the diffuser and peak M_{is} at the lip were comparable between both configurations. Although for separated flows, there was a difference in the incidence angle of about 1° to generate similar flow physics, it was concluded that the installed LLF-DNW intake aerodynamics are representative of those expected in an isolated configuration. This was verified for angles up to 3° above AoA_{crit}.

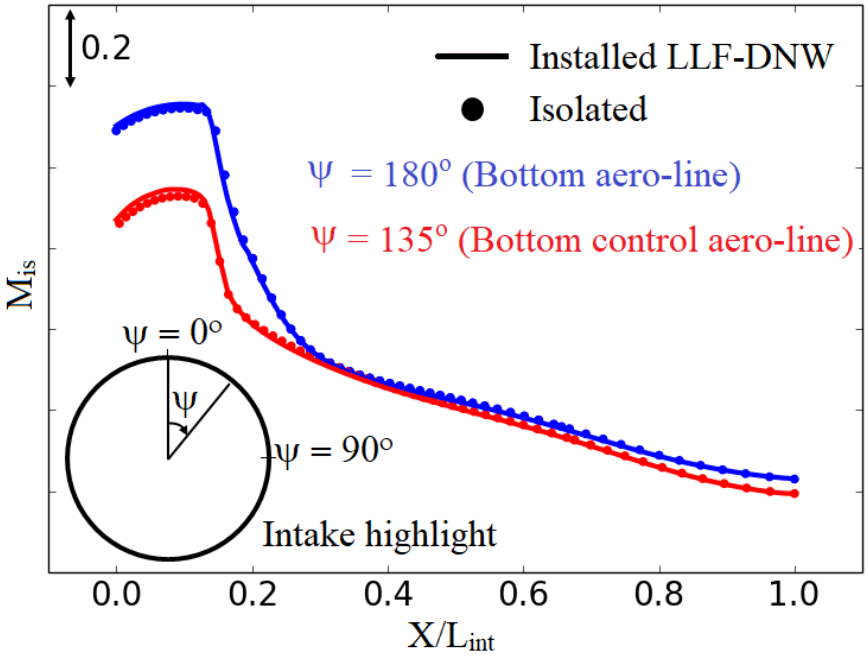

Figure 5. Comparison of isentropic Mach number along intake bottom ($\psi = 180°$) and bottom-control ($\psi = 135°$) aero-lines between isolated and installed LLF-DNW at $MFCR \approx 1.6$ and $AoA = AoA_{crit} - 1°$.

Overall, across the range of angles of attack, similar trends in pressure recovery and swirl angle at the AIP were observed for the isolated and installed arrangements (Figure 6). This representation enables a qualitative representation of the regions with larger flow distortion. As expected, low-pressure regions form at the bottom of the isolated intake at high angles of attack [10]. The installed configuration demonstrated this same behaviour, which confirms that the rig and strut geometries do not introduce significant flow asymmetry or bias towards one side. It is noteworthy that for separated flows, there was a difference in the azimuthal and radial extent of the low-pressure region between both configurations at fixed incidence. To obtain a similar distortion pattern, both configurations need to be at different angles of attack (Figure 7). For example, this is identified when the installed configuration operates at $AoA = AoA_{crit} + 2°$ and the isolated configuration at $AoA = AoA_{crit} + 4°$ (Figure 6). Whilst this shows a slight variation between the two configurations, it also confirms that the installed intake in the LLF-DNW wind tunnel can produce distortion characteristics that are representative of isolated short intakes. A similar comparative analysis was performed for the swirl angle (Figure 6), which revealed the same trends as those observed for pressure recovery.

Lastly, intake distortion metrics were compared between the installed and isolated cases for a range of angles of attack. In particular, the analysis was based on the typical distortion descriptors of DC_{60} (Equation (2)) and PR (Equation (3)) to quantify the total pressure distortion and loss at the AIP. Both metrics were evaluated on a polar grid of 12 rings and 12 rakes to follow typical industrial practice. Although there are limitations in the use of DC_{60} as a distortion metric, it is considered sufficiently useful for this initial study.

$$DC_{60} = \frac{\overline{P_{0,60}} - \overline{P_{0,AIP}}}{\overline{q_{AIP}}} \tag{2}$$

where $P_{0,60}$ is the lowest area-averaged total pressure in a 60° sector at the AIP, $\overline{P_{0,AIP}}$ is the area-averaged total pressure at the AIP, and $\overline{q_{AIP}}$ is the dynamic head at the AIP

$$PR = \frac{\overline{P_{0,AIP}}}{P_{0,WTT}} \tag{3}$$

where $P_{0,WTT}$ is the wind tunnel inlet total pressure.

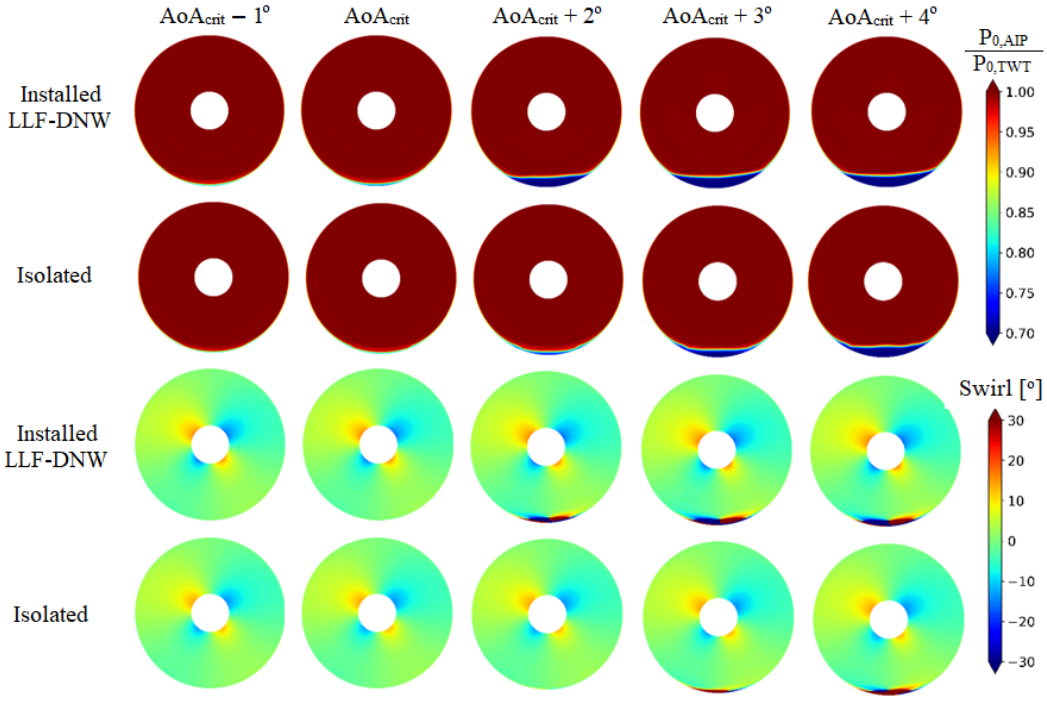

Figure 6. The effect of incidence angle on total pressure recovery (PR) and swirl distortion at the AIP for the installed LLF-DNW and isolated configurations at $MFCR \approx 1.6$.

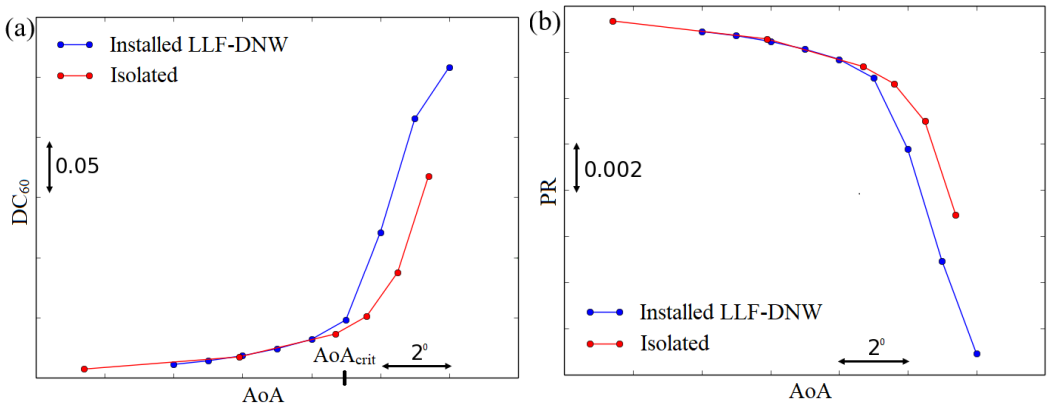

Figure 7. Comparisons of intake distortions metrics between installed LLF-DNW and isolated configurations at $MFCR \approx 1.6$. (**a**) DC_{60}, (**b**) pressure recovery (PR).

Both the installed and isolated configurations exhibit similar values of the distortion coefficient (DC_{60}) and pressure recovery (PR) for angles of attack below the critical incidence of the installed setup (Figure 7). However, as the angle of attack increases, the DC_{60} values are higher and the PR values are lower for the LLF-DNW installed configuration compared with the isolated one. For separated flows, to achieve the same DC_{60} and PR values as in the isolated configuration, the wind tunnel should be operated at an angle of attack that is approximately 1° lower (Figure 7). While this again highlights some discrepancies between the two configurations post-separation, it is important to emphasise that the installed setup in the LLF-DNW is still capable of producing similar flow distortion levels as the isolated case.

These findings provide confidence that the installed configuration will replicate the performance and behaviour of an isolated intake, particularly in terms of isentropic Mach number distribution along the intake, flow characteristics at the AIP, and intake distortion metrics.

3.2. Intake Aerodynamics at High Incidence Angle

Having established confidence that the aerodynamics of the LLF-DNW installed intake are representative of an isolated configuration (Section 3.1), a comprehensive analysis of the intake aerodynamic characteristics was conducted for a range of massflow capture ratios (*MFCRs*) and angles of attack (AoAs). This was carried out for the installed LLF-DNW arrangement to offer insights into the various flow physics that could occur within the intake. This work proposes a taxonomy of flow separation mechanisms that can be used to characterise the flow along the intake (Figure 8). Overall, seven types were identified. Whilst this classification is based on fully turbulent flows, it could be expanded to laminar/turbulent flows. It is expected that the Reynolds number will have an impact on this taxonomy. Although some mechanisms, e.g., fan-induced separation, are not present in this study, they have been described in previous research [4] and are included in this taxonomy for completeness. A closed subsonic lip separation (Type-1 in Figure 8) can occur due to an adverse pressure gradient (APG) [36]. This can change to an open subsonic lip separation (Type-4) for strong APGs. As reported in earlier studies [21,22], shock-induced separation is a common flow separation mechanism in intakes at high incidence. This occurs due to a significant flow acceleration around the lip and can result in a shock-induced separation followed by reattachment (Type-2) or an open separation that extends to the fan (Type-5). When the intake operates at a low massflow capture ratio, adverse flow phenomena can develop in the diffuser (Figure 1), leading to either closed-diffusive separation (Type-3) or open-diffusive separation (Type-6). There could also be a fan-modulated diffusion-driven separation (Type-7), which should be considered in fan–intake coupling studies.

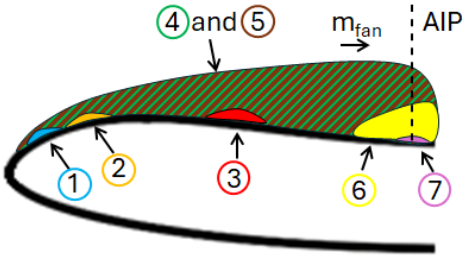

Definition
Type-1: A closed, subsonic lip separation
Type-2: A closed, shock-induced separation
Type-3: A closed, diffusive separation
Type-4: An open, subsonic, lip separation
Type-5: An open, shock-induced, lip separation
Type-6: An open, diffusion-driven, separation
Type-7: A fan-modulated, diffusion-driven separation

Figure 8. Flow separation taxonomy for characterising the intake characteristics. The same colour code is used in Figure 9.

To provide a more comprehensive understanding of the underlying flow physics encountered throughout the aerodynamic operating conditions, Figure 10 shows the pressure recovery distribution at the AIP, as well as the isentropic Mach number and axial wall shear stress variation along the lower intake aero-line. Four representative operating conditions were selected, each corresponding to one of the flow separation mechanisms previously identified in Figure 9. These cases successfully capture the changes in the intake flow physics in the aerodynamic design space and the impact on the distortion characteristics.

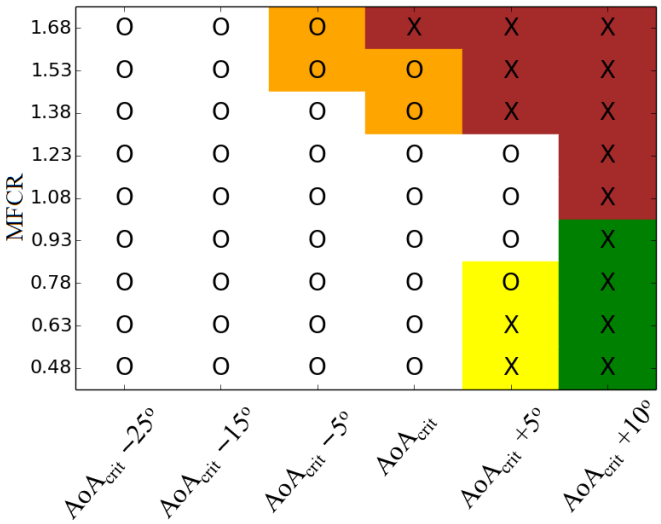

Figure 9. The categorisation of the intake flow characteristics with the proposed taxonomy across the *MFCR*-AoA aerodynamic design space. The white colour refers to attached flow. The symbols ○ and × are for $DC_{60} < DC_{60,ref}$ and $DC_{60} > DC_{60,ref}$, respectively. The same colour code is used in Figure 8.

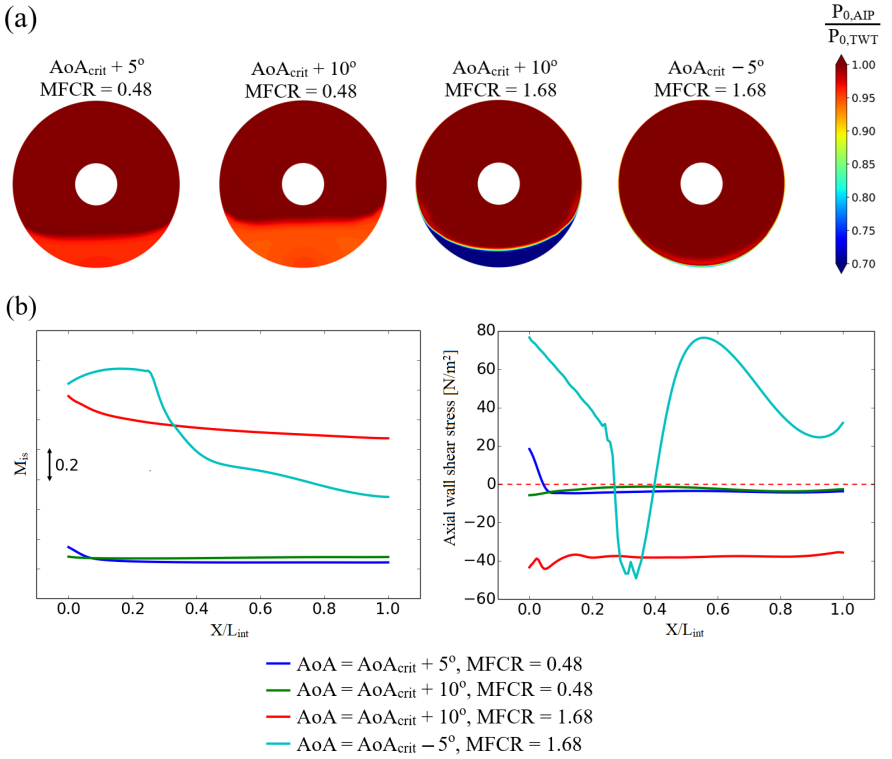

Figure 10. Changes on the intake flow characteristics across aerodynamic design space. (**a**) AIP plane, (**b**) Intake bottom aero-line. The red dotted line shows the value of axial wall shear stress equal to zero.

The intake aerodynamics in the installed LLF-DNW configuration were assessed across a range of *MFCRs* from 0.48 to 1.68 and angles of attack from $AoA = AoA_{crit} - 25°$ to $AoA_{crit} + 10°$, where AoA_{crit} is the critical angle at $MFCR \approx 1.6$. Overall, 54 installed aspirated cases were computed using a full-factorial approach with 6 different values of incidence and 9 *MFCRs*. Based on a traditional DC_{60} threshold ($DC_{60,ref}$) for acceptable flow distortion, the *MFCR*-AoA aerodynamic space was identified (Figure 9). The intake

aerodynamics are benign at angles of attack lower than $AoA = AoA_{crit}$ across the range of $MFCRs$ considered, and therefore, DC_{60} was below $DC_{60,ref}$ (Figure 9). As the incidence angle increases to $AoA = AoA_{crit}$, the only massflow capture ratio ($MFCR$) at which DC_{60} exceeds the reference value ($DC_{60,ref}$) is $MFCR$ = 1.68. This flow distortion is attributed to an open shock-induced lip separation, classified as Type-5 (Figure 8) in the proposed taxonomy. For this incidence angle, there is also closed shock-induced lip separation (Type-2) for $MFCR$ = 1.53 and 1.38, in which the length of the separation bubble is approximately 15% and 1% of L_{int}, respectively. However, this flow separation is insufficient to cause significant flow disturbances, and therefore, DC_{60} is below the reference value.

To provide insights into the intake flow characteristics as a function of the $MFCR$, Figure 11 presents the isentropic Mach number (M_{is}) and axial wall shear stress distributions along the bottom aero-line at fixed $AoA = AoA_{crit}$. For $MFCRs$ below 1.23, the flow experiences a modest acceleration along the lip, which leads to relatively benign M_{is} distributions. However, as the massflow capture ratio increases to $MFCR$ = 1.38, the stronger flow acceleration around the lip terminates in shock-induced separation and reattachment (Figure 11b). At a higher $MFCR$ of 1.53, both the peak and pre-shock M_{is} increase relative to $MFCR$ = 1.38 by $\Delta M_{is} = 0.23$ and $\Delta M_{is} = 0.19$, respectively. This results in the previous described larger flow separation (Type-2 in Figure 8) that changes from approximately 1% to 15% of the intake length. For $MFCR$ = 1.68, there is a high value of pre-shock M_{is} which induces an open shock-induced separation (Type-5 in Figure 8). As the angle of attack is further increased to $AoA = AoA_{crit} + 5°$, various flow phenomena emerge along the intake. For relatively low massflow capture ratios ($MFCRs < 0.8$), open diffusive-driven separation occurs (Type-6 in Figure 8), which results in $DC_{60} > DC_{60,ref}$. As the $MFCR$ increases, the flow reattaches, and DC_{60} falls below the reference threshold up to MFCR = 1.23. However, with a further increase in the $MFCR$, an open shock-induced separation at the intake lip is observed (Type-5). This highlights the complexity of flows that can arise in an intake at high incidence angles and how high levels of distortion can be produced by different flow physics. Finally, a further increment in the incidence to $AoA = AoA_{crit} + 10°$ results in DC_{60} values above the reference ($DC_{60,ref}$) across the range of $MFCRs$ considered. For this angle of attack, the flow is fully separated along the intake. For an $MFCR < 1$, the flow separation mechanism is Type-4, i.e., open subsonic lip separation. As the $MFCR$ increases above 1.0, the mechanism changes to an open shock-induced separation (Type-5).

This analysis highlighted a variety of flow separation mechanisms that can occur in an intake at high angles of attack. Whilst this taxonomy was considered for RANS simulations, it forms a basis for the analysis of future unsteady simulations, contributing to a deeper understanding of fan/intake interactions.

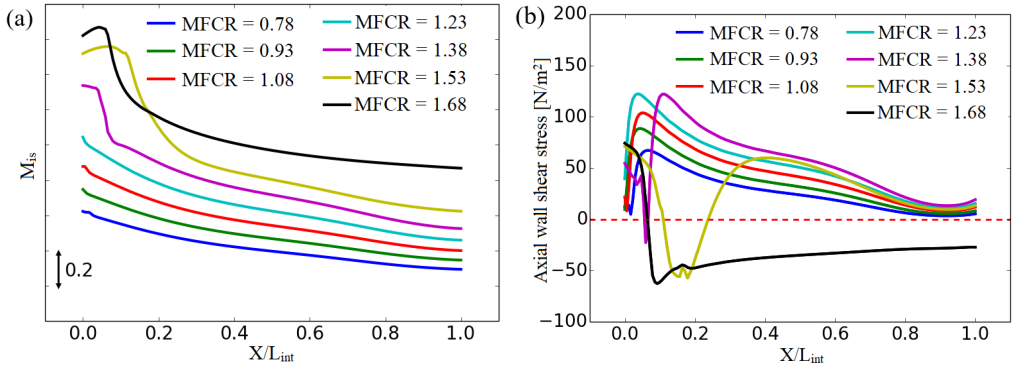

Figure 11. Effect of $MFCR$ on aerodynamics of bottom aero-line at $AoA = AoA_{crit}$. (**a**) Isentropic Mach number, (**b**) axial wall shear stress. The red dotted line shows the value of axial wall shear stress equal to zero.

3.3. Full-Annulus Installed Computations

The effect of fan integration in flow separation over the intake was examined using a fan–intake coupled analysis with full-annulus computations and the harmonic mixing plane method. For this study, two massflow capture ratios of about 1.0 and 1.5 were selected. At $MFCR \approx 1.0$, the flow is primarily governed by diffusion-driven separation, while at a higher $MFCR$ of approximately 1.5, shock-induced separation dominates. This allows for a comprehensive investigation of fan/intake coupling and its effect on both flow separation mechanisms.

Figure 12 compares the distortion metrics of DC_{60} and PR for the aspirated and fan/intake coupled configurations at both $MFCRs$. As expected, the critical angle at which DC_{60} exceeds $DC_{60,ref}$ is lower for the higher $MFCR$ of 1.5. For both $MFCRs$, the fan/intake interaction increases the critical angle by approximately 1° relative to the aspirated configuration. For the aspirated setup, there is a significant increase in DC_{60} between the critical angle and an additional 1°, with changes of approximately $\Delta DC_{60} = 0.40$ for an $MFCR \approx 1.0$ and $\Delta DC_{60} = 0.13$ for an $MFCR \approx 1.5$. The flow distortion is reduced due to the fan/intake coupling effect [10,15], and the critical angle increases by approximately 1°. For separated flows, the same level of DC_{60} between aspirated and fan/intake coupled configurations can be achieved with an incidence approximately 1° larger in the coupled arrangement. A similar conclusion was derived from the distortion metric of PR (Figure 12). It is worth mentioning that as part of this pre-test CFD campaign, a range of massflow and incidence angles was considered to map out the aerodynamic design space. This resulted in significant changes in the intake flow physics (Figure 11) and distortion levels (Figure 12). The DC60 values are relatively high for some conditions where the intake flow is fully separated (Figure 12). However, one of the aims of the experiment is to investigate the effect of high levels of distortion. As such, these conditions will also be of interest to characterise the fan's performance and stability margin under a comprehensive range of non-uniform inflow conditions.

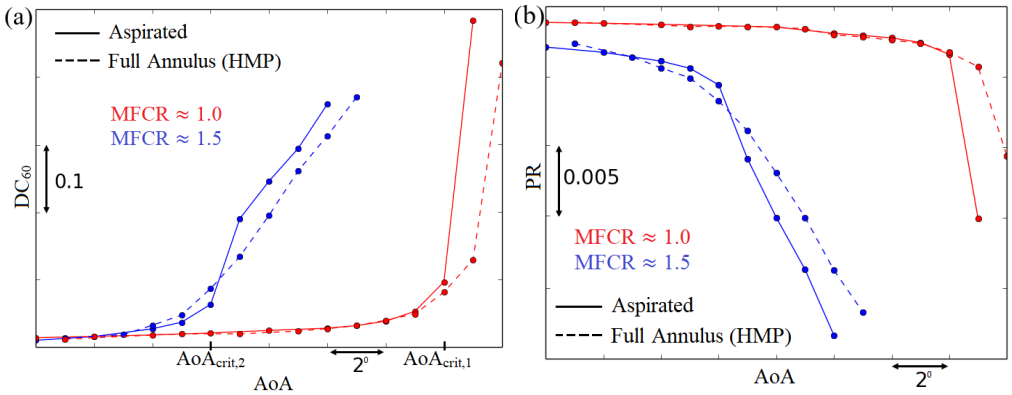

Figure 12. Impact of fan suppression on intake distortion metrics. (**a**) DC_{60}, (**b**) pressure recovery (PR).

The differences in the integral distortion metrics (Figure 12) are caused by changes in the intake aerodynamics (Figure 13). For the aspirated case and an $MFCR$ of 1.0, there are flow separation mechanisms of Type-1 and Type-6 (Figure 8). The extension of flow separation is identified with an axial wall shear stress of zero (represented by the pink iso-line in Figure 13). It is important to emphasise that this serves as an indicator of separation but does not provide a definitive criterion for three-dimensional flows. As the incidence is increased by 1°, i.e., $AoA = AoA_{crit,1} + 1°$, both separation topologies remain, but the diffusion-driven one enlarges considerably, which results in the large distortion observed in the DC_{60} and PR metrics (Figure 12). The fan interaction suppresses some of the diffusion-driven separation (Figure 13). To obtain similar flow separation characteristics

to those of the isolated case at $AoA = AoA_{crit,1} + 1°$, the fullannulus operates at 1° higher, i.e., $AoA = AoA_{crit,1} + 2°$. For an $MFCR \approx 1.5$, there is shock-induced separation and reattachment (Type-2 in Figure 8) at $AoA = AoA_{crit,2}$ in the aspirated case. With an increment of 1°, the shock strength increases, and the separation topology changes to open shock-induced separation (Type-5 in Figure 8). It is worth highlighting that for this angle of attack ($AoA = AoA_{crit,2} + 1°$), the full annulus calculations with the HMP method also show an open shock-induced separation, i.e., Type-5. Overall, it is observed that the flow aerodynamics along the intake are broadly similar between the aspirated cases and full annulus calculations with an offset in the incidence angle due to the effect of fan suppression.

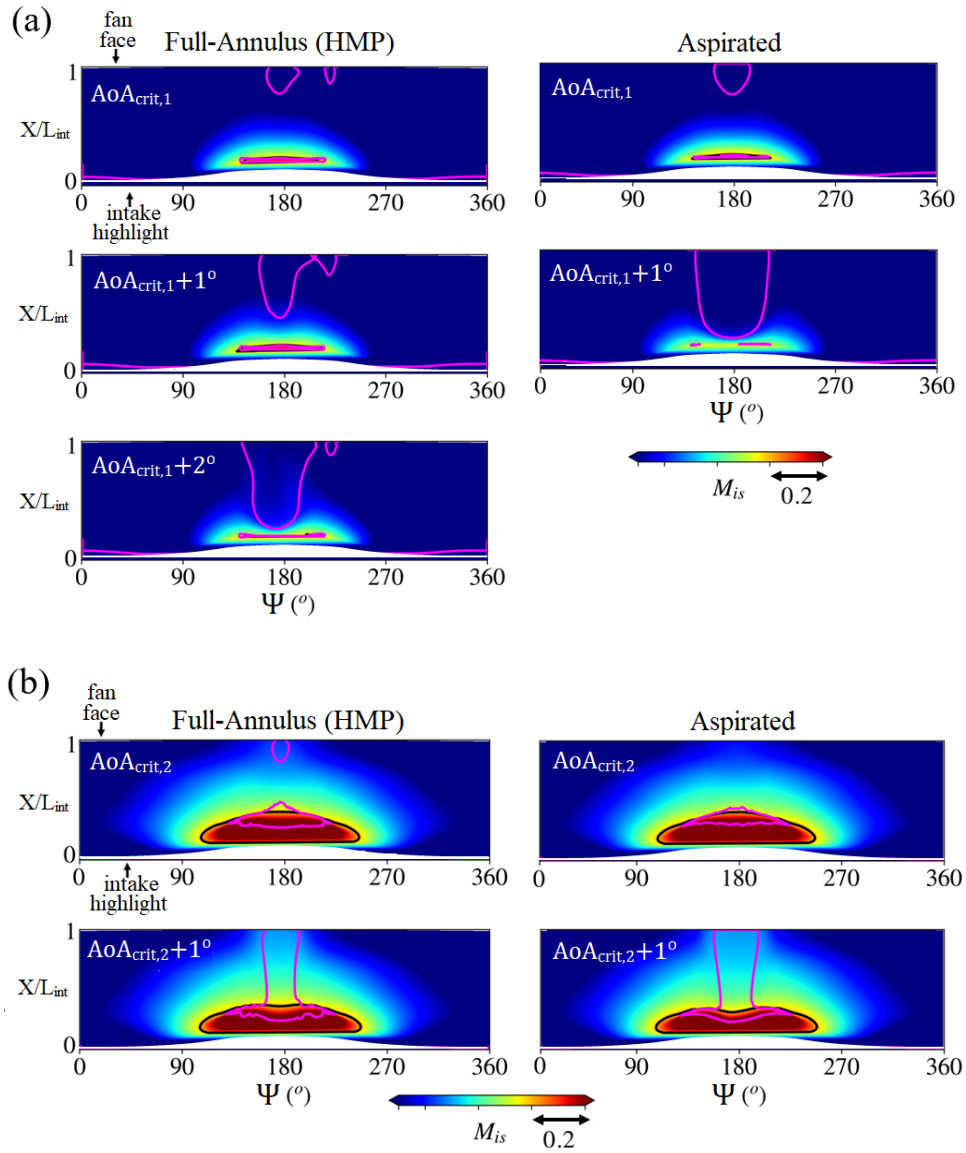

Figure 13. Unwrapped surfaces of intake coloured by isentropic Mach number distribution. Black iso-lines are for M_{is} = 1, and pink iso-lines are for axial wall shear stress of 0. (**a**) $MFCR \approx 1.0$, (**b**) $MFCR \approx 1.5$.

The changes in distortion metrics (Figure 12) and isentropic Mach number distributions (Figure 13) are linked to the flow characteristics at the AIP (Figure 14). For example, for $MFCR \approx 1.0$, the sudden increase in DC_{60} of the isolated arrangement when the incidence angle changes from $AoA_{crit,1}$ to $AoA_{crit,1} + 1°$ is related to the considerable large increment in the radial and azimuthal low-pressure region in the bottom half (Figure 14a). This

increment is more gradual for the full annulus computations, which highlights the effect of fan suppression for conditions that are dominated by diffusion-driven separation. Similar findings were observed for the $MFCR \approx 1.5$ (Figure 14b). For the aspirated case, there is a significant increase in the low-pressure regions when the angle of attack changes from $AoA_{crit,2}$ to $AoA_{crit,2} + 1°$. The increase in the low-pressure region is also more gradual for the coupled configuration, which is aligned with previous observations [16,18].

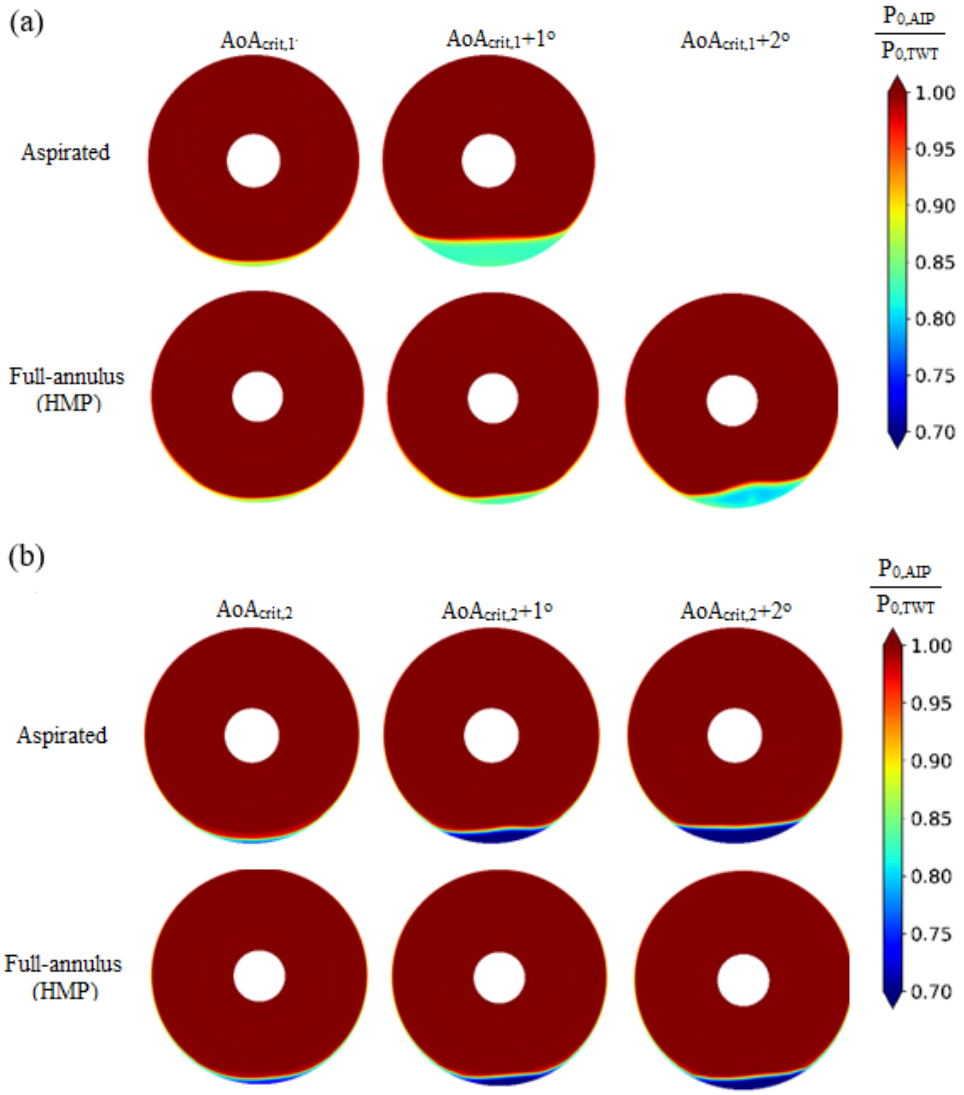

Figure 14. The effect of incidence angle on total pressure recovery (PR) at the AIP for the aspirated and full annulus (HMP) configurations. (**a**) $MFCR \approx 1.0$, (**b**) $MFCR \approx 1.5$.

It is important to note that whilst this work was based on the RANS k-ω SST [29] turbulence closure, it is envisaged that there is a sensitivity to the turbulence model. For example, Carnevale et al. [37] investigated the effect of turbulence model intake distortion under high-incidence conditions. Overall, it was concluded that the critical angle could change by approximately 1° between Spalart–Allmaras and k-ω SST, in which the two-equation closure had a better agreement with experimental data and post-separation characteristics. We also acknowledge the need to quantify the possible uncertainty of these predictions relative to other CFD modelling approaches such as URANS and LES. Cao et al. [10] compared steady RANS coupled with a body force fan model and full annulus URANS for a separated intake case at high incidence. It was found that the steady

RANS method had the same DC60 as the URANS case at only 1 degree of incidence lower. This difference is attributed to both the inherent unsteadiness captured by URANS and the difference in fan representation. High-fidelity LES computations for the investigation of shock wave boundary layer interactions in an aspirated intake were performed by Ma et al. [38] as well as Kalsi and Tucker [39]. Relative to LES, it was concluded that steady RANS presented larger lengths of flow separation, i.e., flow reattachment was delayed. However, it is important to note that Ma et al. [38] also reported that the differences between RANS and LES in reattachment characteristics were significantly reduced when the calculation includes the stabilising effect of the fan. These studies did not investigate the impact of CFD fidelity in the onset of flow separation as a function of incidence angle. Overall, there is not a clear conclusion in the current literature about the impact of CFD fidelity on intake distortion characteristics. This is an area of future work, and the novel experimental data that will be collected as part of this test campaign will enable us to derive CFD modelling guidelines for short aero-engine intakes.

4. Conclusions

This study evaluates the aerodynamics of a compact aero-engine intake designed for a new rig, which will be tested at the Large Low-Speed Facility of the German-Dutch Wind Tunnels (LLF-DNW). A range of computations were performed to quantify the aerodynamic differences in the intake for the isolated and installed LLF-DNW configurations. This work was based on high-incidence conditions. Overall, it was predicted that the LLF-DNW test campaign will provide representative flows of an equivalent isolated intake and is suitable for this challenging design space. The intake aerodynamics in the installed LLF-DNW configurations are representative of the equivalent isolated case in terms of isentropic Mach number distributions along the intake, distortion characteristics at the AIP, and integral distortion metrics. A flow separation taxonomy for classifying the flow along the intake was proposed and used to provide insights into the expected flow physics during the test campaign.

Initial installed fan/intake coupled simulations were performed with full annulus computations and a harmonic mixing plane approach, revealing that the critical angle can be increased by approximately 1° relative to the aspirated configuration. This is aligned with previous work, where the change in critical angle between aspirated and intake/fan coupled configurations changed from 1° [16] to 5° [10]. This range can be caused by differences in intake shapes and the associated aerodynamics or the numerical modelling approaches. Therefore, future work should focus on the validation of numerical methods for aero-engine intake applications. Overall, this work provides an initial evaluation of the aerodynamics of the novel intake/fan LLF-DNW test rig, provides guidance for wind tunnel testing, and lays a foundation for subsequent unsteady coupled intake/fan studies.

Author Contributions: Conceptualisation, F.T. and D.M.; methodology, F.T. and Y.F.M.; software, F.T., J.H.-R. and Y.F.M.; validation, F.T. and Y.F.M.; formal analysis, F.T., D.M. and J.H.-R.; investigation, F.T., D.M., J.H.-R., Y.F.M. and I.B.; resources, F.T., D.M., J.H.-R., Y.F.M. and I.B.; data curation, F.T.; writing—original draft preparation, F.T.; writing—review and editing, F.T., D.M., J.H.-R., Y.F.M. and I.B.; visualisation, F.T.; supervision, D.M. and I.B.; project administration, D.M. and I.B.; funding acquisition, D.M. and I.B. All authors have read and agreed to the published version of the manuscript.

Funding: This research was funded in scope of the 6th Federal Aeronautical Research Program (LuFo VI-1) by the German Federal Ministery of Economic Affairs and Climate Action (BMWK, formerly BMWi) and is part of the project ModeGo (FKZ: 20T1914A).

Data Availability Statement: The datasets presented in this article are not readily available because of an existing confidentiality agreement. Requests to access the datasets should be directed to f.tejero@cranfield.ac.uk.

Conflicts of Interest: Authors Yuri Frey Marioni and Ian Bousfield were employed by the company Rolls-Royce. The remaining authors declare that the research was conducted in the absence of any commercial or financial relationships that could be construed as a potential conflict of interest.

Nomenclature and Abbreviations

The following nomenclature, subscripts, and abbreviations are used in this manuscript:

Nomenclature	
A	Area
D	Diameter
DC_{60}	Total pressure distortion metric
in	Inches
L	Length
M	Mach number
ψ	Intake aero-line
Subscripts	
crit	Critical
crit,1	Critical at $MFCR \approx 1.0$
crit,2	Critical at $MFCR \approx 1.5$
hi	Highlight
int	Intake
is	Isentropic
ref	Reference
0	Total
∞	Inlet working section
Abbreviations	
AIP	Aerodynamic interface plane
AoA	Angle of attack
HMP	Harmonic mixing plane
LLF-DNW	Large Low-Speed Facility of the German Dutch Wind Tunnels
$MFCR$	Massflow capture ratio
WT	Wind tunnel

References

1. Birch, N. 2020 Vision: The Prospects for Large Civil Aircraft Propulsion. *Aeronaut. J.* **2000**, *104*, 347–352. [CrossRef]
2. Daggett, D. *Ultra-Efficient Engine Technology Systems Integration and Environmental Assessment*; Technical Report CR-2002-211754; NASA: Washington, DC, USA, 2002.
3. Daggett, D.; Brown, S.; Kawat, R. *Ultra-Efficient Engine Diameter Study*; Technical Report CR-2003-212309; NASA: Washington, DC, USA, 2003.
4. Boscagli, L.; MacManus, D.; Christie, R.; Sheaf, C. Effect of Unsteady Fan-Intake Interaction on Short Intake Design. *J. Eng. Gas Turbines Power* **2023**, *146*, 031008. [CrossRef]
5. Sanchez-Moreno, F.; MacManus, D.; Hueso-Rebassa, J.; Tejero, F.; Matesanz-Garcia, J.; Sheaf, C. Optimization of Installed Compact and Robust Nacelles Using Surrogate Models. In Proceedings of the 33rd Congress of the International Council of the Aeronautical Sciences: ICAS 2022, Stockholm, Sweden, 4–9 September 2022.
6. Hueso-Rebassa, J.; MacManus, D.; Tejero, F.; Goulos, I.; Sánchez-Moreno, F.; Sheaf, C. Design Optimisation of Non-Axisymmetric Exhausts for Installed Civil Aero-Engines. *Aerosp. Sci. Technol.* **2023**, *142*, 108700. [CrossRef]
7. Tejero, F.; MacManus, D.; Goulos, I.; Sheaf, C. Propulsion Integration Study of Civil Aero-Engine Nacelles. *Aeronaut. J.* **2023**, *128*, 325–339. [CrossRef]
8. Tejero, F.; MacManus, D.; Heidebrecht, A.; Sheaf, C. Artificial Neural Network for Preliminary Design and Optimisation of Civil Aero-engine Nacelles. *Aeronaut. J.* **2024**, *128*, 2261–2280. [CrossRef]

9. Abdul-Kaiyoom, M.; Lamkin, A.; Yildrim, A.; Gray, J.S.; Mader, C.A.; Martins, J. Coupled Aeropropulsive Design Optimization of a Podded Electric Propulsor. *Struct. Multidiscip. Optim.* **2025**, *68*, 13. [CrossRef]
10. Cao, T.; Vadlamani, N.R.; Tucker, P.G.; Smith, A.R.; Slaby, M.; Sheaf, C. Fan–Intake Interaction Under High Incidence. *J. Eng. Gas Turbines Power* **2016**, *139*, 041204. [CrossRef]
11. Boscagli, L.; Christie, R.; MacManus, D.; Piovesan, T. Aerodynamics of a short intake in crosswind. *Aerosp. Sci. Technol.* **2022**, *129*, 107826. [CrossRef]
12. Reid, C. The Response of Axial Flow Compressors to Intake Flow Distortion. In Proceedings of the ASME 1969 Gas Turbine Conference and Products Show, Cleveland, OH, USA, 9–13 March 1969; p. V001T01A029.
13. Ma, Y.; Cui, J.; Vadlamani, N.R.; Tucker, P. Effect of Fan on Inlet Distortion: Mixed-Fidelity Approach. *AIAA J.* **2018**, *56*, 2350–2360. [CrossRef]
14. Burlot, A.; Sartor, F.; Vergez, M.; Meheut, M.; Barrier, R. Method Comparison for Fan Performance in Short Intake Nacelle. In Proceedings of the 2018 Applied Aerodynamics Conference, Atlanta, GA, USA, 25–29 June 2018; AIAA Paper 2018-4204.
15. Peters, A.; Spakovszky, Z.S.; Lord, W.K.; Rose, B. Ultrashort Nacelles for Low Fan Pressure Ratio Propulsors. *J. Turbomach.* **2014**, *137*, 021001. [CrossRef]
16. Kennedy, S.; Robinson, T.; Spence, S.; Richardson, J. Computational Investigation of Inlet Distortion at High Angles of Attack. *J. Aircr.* **2014**, *51*, 361–376. [CrossRef]
17. Silva, V.T.; Lundbladh, A.; Petit, O.; Xisto, C. Multipoint Aerodynamic Design of Ultrashort Nacelles for Ultrahigh-Bypass-Ratio Engines. *J. Propuls. Power* **2022**, *38*, 541–558. [CrossRef]
18. Carnevale, M.; Wang, F.; Green, J.S.; Mare, L.D. Lip Stall Suppression in Powered Intakes. *J. Propuls. Power* **2016**, *32*, 161–170. [CrossRef]
19. Magrini, A.; Benini, E. Study of Geometric Parameters for the Design of Short Intakes with Fan Modelling. *Chin. J. Aeronaut.* **2022**, *35*, 18–32. [CrossRef]
20. Gunn, E.J.; Brandvik, T.; Wilson, M.J. Fan-Intake Coupling with Conventional and Short Intakes. In *Turbo Expo: Power for Land, Sea, and Air*; Volume 1: Aircraft Engine; Fans and Blowers; Marine; Wind Energy; Scholar Lecture; American Society of Mechanical Engineers: New York, NY, USA, 2021; p. V001T01A003.
21. Coschignano, A.; Babinsky, H. Influence of Near-Leading Edge Curvature on the Performance of Aero-Engine Intake Lips at High-Incidence. In Proceedings of the 34th AIAA Applied Aerodynamics Conference, Washington, DC, USA, 13–17 June 2016; AIAA Paper 2016-3559.
22. Coschignano, A.; Atkins, N.; Babinsky, H.; Serna, J. Effect of Reynolds Number on a Normal Shock Wave-Transitional Boundary-Layer Interaction over a Curved Surface. *Exp. Fluids* **2019**, *60*, 185. [CrossRef]
23. Hodder, B.K. *An Investigation of Engine Influence on Inlet Performance*; Technical Report NASA CR-166136; NASA: Washington, DC, USA, 1981.
24. Tejero, F.; MacManus, D.; Hueso-Rebassa, J.; Frey, Y.; Bousfield, I. Aerodynamics of a Short Intake at High Incidence. In Proceedings of the 16th European Turbomachinery Conference, ETC2025, Hannover, Germany, 24–25 March 2025; Paper ETC2025-298.
25. Greitzer, E.M.; Mazzawy, R.S.; Fulkerson, D.A. Flow Field Coupling Between Compression System Components in Asymmetric Flow. *J. Eng. Power* **1978**, *100*, 66–72. [CrossRef]
26. Roache, P. A Method for Uniform Reporting of Grid Refinement Studies. *J. Fluids Eng.* **1994**, *116*, 405–413. [CrossRef]
27. Mohankumar, B.; Hall, C.; Wilson, M. Fan Aerodynamics With a Short Intake at High Angle of Attack. *J. Turbomach.* **2021**, *143*, 051003. [CrossRef]
28. Moinier, P. Algorithm Developments for an Unstructured Viscous Flow Solver. Ph.D. Thesis, University of Oxford, Oxford, UK, 1999.
29. Menter, F.R. Two-Equation Eddy-Viscosity Turbulence Models for Engineering Applications. *AIAA J.* **1994**, *32*, 1598–1605. [CrossRef]
30. Crumpton, P.I.; Moinier, P.; Giles, M.B. An Unstructured Algorithm for High Reynolds Number Flows on Highly Stretched Grids. In Proceedings of the 10th International Conference on Numerical Methods for Fluid Dynamics, Swansea, UK, 21–25 July 1997.
31. Misev, C.; Hills, N.J. Steepest Descent Optimisation of Runge–Kutta Coefficients for Second Order Implicit Finite Volume CFD Codes. *J. Comput. Phys.* **2018**, *354*, 576–592. [CrossRef]
32. Sutherland, W. The Viscosity of Gases and Molecur Force. *Philos. Mag.* **1893**, *5*, 507–531. [CrossRef]
33. Amirante, D.; Ganine, V.; Hills, N.; Nicholas, J.; Adami, P. A Coupling Framework for Multi-Domain Modelling and Multi-Physics Simulations. *Entropy* **2021**, *23*, 758. [CrossRef] [PubMed]
34. Ganine, V.; Amirante, D.; Hills, N. Enhancing Performance and Scalability of Data Transfer Across Sliding Grid Interfaces for Time-Accurate Unsteady Simulations of Multistage Turbomachinery Flows. *Comput. Fluids* **2015**, *115*, 140–153. [CrossRef]
35. Pullan, G.; Adamczyk, J.J. Filtering Mixing Planes for Low Reduced Frequency Analysis of Turbomachines. *J. Turbomach.* **2017**, *139*, 091009. [CrossRef]

36. Mottaghian, P.; Yuan, J.; Piomelli, U. Boundary Layer Separation Under Strong Adverse Pressure Gradient over Smooth and Rough Walls. In *Proceedings of the Direct and Large-Eddy Simulation X*; Springer International Publishing: Cham, Switzerland, 2018; pp. 173–179.
37. Carnevale, M.; Wang, F.; di Mare, L. Low Frequency Distortion in Civil Aero-engine Intake. *J. Eng. Gas Turbines Power* **2016**, *139*, 041203. [CrossRef]
38. Ma, Y.; Vadlamani, V.R.; Cui, J.; Tucker, P. Comparative Studies of RANS Versus Large Eddy Simulation for Fan–Intake Interaction. *J. Fluids Eng.* **2018**, *141*, 031106. [CrossRef]
39. Kalsi, H.S.; Tucker, P.G. Numerical Modelling of Shock Wave Boundary Layer Interactions in Aero-Engine Intakes at Incidence. In Proceedings of the ASME Turbo Expo 2018: Turbomachinery Technical Conference and Exposition, Oslo, Norway, 11–15 June 2018; Volume 1: Aircraft Engine; Fans and Blowers; Marine.

Disclaimer/Publisher's Note: The statements, opinions and data contained in all publications are solely those of the individual author(s) and contributor(s) and not of MDPI and/or the editor(s). MDPI and/or the editor(s) disclaim responsibility for any injury to people or property resulting from any ideas, methods, instructions or products referred to in the content.

https://dspace.org/

Aerodynamics of short intake at high incidence

Tejero, Fernando; MacManus, David G.; Hueso Rebassa, Josep; Frey Marioni, Yuri; Bousfield, Ian

2026-03
MDPI
https://doi.org/10.3390/ijtpp11010006
Tejero F, MacManus D, Hueso-Rebassa J, et al., (2026) Aerodynamics of short intake at high incidence. International Journal of Turbomachinery, Propulsion and Power, Volume 11, Issue 1, March 2026, Article number 6

Downloaded from a DSpace repository. https://dspace.org/